TISSUE ENGINEERING: Part A
Volume 20, Numbers 5 and 6, 2014

DOI: 10.1089/ten.tea.2013.0277

Fabrication and Evaluation of PLLA Multichannel Conduits with Nanofibrous Microstructure for the Differentiation of NSCs *In Vitro*

Chen-guang Zeng, PhD,[1] Yi Xiong, PhD,[2] Gaoyi Xie, PhD,[1] Peng Dong, BS,[1] and Daping Quan, PhD[1]

Nerve conduits (NCs) with multiple longitudinally aligned channels, being mimicking the natural nerves anatomical structure, have been attracted more and more attentions. However, some specific structural parameters of a conduit that would be beneficial for further improvement of neural tissue regeneration were not comprehensively considered. Using a systematized device and combining low-pressure injection molding and thermal-induced phase separation, we fabricated 33-channel NCs (outer diameter 3.5 mm, channel diameter 200 μm) with different well-defined microscopic features, including NCs with a nano-fibrous microstructure (NNC), NCs with microspherical pores and nano-fibrous pore walls (MNC), and NCs with a ladder-like microstructure (LNC). The porosities of these NCs were ~90% and were independent of the fine microstructures, whereas the pore size distributions were clearly distinct. The adsorption of bovine serum albumin for the NNC was a result of having the highest specific surface area, which was 3.5 times that of the LNC. But the mechanical strength of NNC was lower than that of two groups because of a relative high crystallinity and brittle characteristics. *In vitro* nerve stem cells (NSCs) incubation revealed that 14 days after seeding the NSCs, 31.32% cells were Map2 positive in the NNC group, as opposed to 15.76% in the LNC group and 23.29% in the MNC group. Addition of NGF into the culture medium, being distinctive specific surface area and a high adsorption of proteon for NNC, 81.11% of neurons derived from the differentiation of the seeded NSCs was obtained. As a result of imitating the physical structure of the basement membrane of the neural matrix, the nanofibrous structure of the NCs has facilitated the differentiation of NSCs into neurons.

Introduction

Nerve conduits (NCs) fabricated from synthetic or natural materials have been widely applied in nerve regeneration. Serving as artificial extracellular matrixes and regulative/stimulative signal vehicles, NCs have been designed to provide protection, guidance, and bridging to the damaged nerve.[1–4] A effective strategy was that, referred to the mechanism of contact guidance effect, which commonly exists in the embryo development and body function maintaining, the specific structural feature of the scaffold was set to become physical cues for tissue/cells, so that the cell behavior and fate could be regulated or controlled in a way.[5–7]

The geometric tubular structure, which can be considering as evolving from the shape of natural endoneurium, perineurium, and epineurium, has been adopted to promote the growing, spreading, and functioning of neurons, which was manifested in the researches of single-channel NCs for neural tissue engineering in the early stages[8–11] and the later multichannel NCs.[12–23] These conduits maintained specific guidance cues for the regenerated axons or fasciculus in *in vitro* cell culture, the *in vivo* rat sciatic nerve injury model, and the total-transected spinal cord grafts model. Li[24] summarized the effect of these guidance channels in his review. In the sight of the technique, however, the current fabrication methods for NCs with multiple longitudinally aligned channels, including injection molding,[11–13] casting,[8,25,26] wire heating,[15] mandrel/fiber removal,[14,16,20,21,27,28] membrane rolling-up,[29–32] and immersion precipitation,[33] have remained unsatisfactory with respect to the sufficient number of appropriately sized channels in the conduits for the formation of bands of Bungner. Meanwhile, little attention has been paid to the microstructure between the channels, which may affect the communication of nerve cells and the formation of neural networks *in vitro* or *in vivo*.

In fact, the basement membrane of the neural matrix is composed of nanofibrils with a diameter of 50 to 500 nm in addition to the multiple basal lamina tubes. In some mimic models, researchers[34–37] have reported the effects of the nanofibrous structure of matrices on the neuron cell attachment, proliferation, and differentiation. However, these matrices

[1]DSAPM and PCFM Lab, School of Chemistry and Chemical Engineering, Sun Yat-Sen University, Guangzhou, China.
[2]Shenzhen-PKU-HKUST Medical Center, Biomedical Research Institute, Shenzhen, China.

were only a two-dimensional (2D) structure with tunable nanoscale fibers, which were prepared using electrospinning, self-assemble, and microfluid techniques. Particularly, an aligned nanofibrils on the inner luminal surface of the single-channel conduit was fabricated by the electrospinning method,[27] in fact, the cells planted in the conduit were still limited in a 2D-scale microenvironment. As approaching to the practical microenvironment of cell growth, a three-dimensional (3D) scaffold with a nanofibrous structure was produced using the thermal-induced phase separation (TIPS)[38] combined with a low injection molding technology in this article. Therefore, it is possible to fabricate a neural conduit that possesses multiple basal lamina tubular structures and a nanofibrous architecture, simultaneously. The key problems in this complex technology lie in the mold design and the control of phase separation processes because the number, size, and distribution of channels within the conduit were determined by the precision of the desired molds, and the microstructure in the surface lumen and between the channels was related to the selected solvent, the concentration of the polymer solution, the temperature, and the quenching depth of TIPS. Although it has just been reported that a seven-channel conduit with nanofibrous structure was fabricated,[39] there have not been enough evidences to prove that the microstructure in the NC affected the properties of tubes, especially impacted the fate of seed cells. In addition, there are certain difficulties in technology to fabricate as much as possible channels in the conduit.

The goal of this article was to develop a systematized device to fabricate poly(L-lactide) (PLLA) NCs with both 33 channel-orientation function and ECM biomimetic microstructure on the millimeter and nanometer scales by retrofitting our previous injection mold[22] and adding a heat transfer and nonsolvent exchange system. Two other typical micromorphologies of ladder-like microstructure and macroporous/nano-wall microstructure in the 33-channel conduits can be constructed conveniently by altering the temperature condition and solvent components of TIPS, using the systematized device, as control. Furthermore, the influences of the microstructure on the porosity, mechanical strength, the specific surface area, and the adsorption of bovine serum albumin (BSA) of the conduits were evaluated in detail. Finally, the differentiation of nerve stem cells (NSCs) seeded on the conduits was also evaluated in the presence of NGF or not.

Materials and Methods

Materials

PLLA was purchased from Purasorb® (PL18), and its intrinsic viscosity number (η) was 2.49, the reason for selecting PLLA with high molecular weight is that the degradation rate of PLLA scaffold with nanofibrous structure was much more fast than that of PLLA film or scaffold with porous structure.[40] Diethylene dioxide (1,4-dioxane) and tetrahydrofuran (THF) were of analytical grade and used directly without any additional purification. Ni-Ti alloy wires were purchased from Baoji First Titanium Industry Co., Ltd.

Equipment

The mold, which consisted of mold cavities and wire-supported perforated sheets, was processed by Red Valley Precision Industries Co., Ltd. The temperature control system consisted of a cooling oil circulator (LAUDA Proline RP890; LAUDA DR. R. WOBSER GMBH & CO. KG), a platinum thermocouple, and a cold trap. The infusion system included a peristaltic pump (BQ50-1J; Baoding Longer Precision Pump Co., Ltd.), a fluid switcher, and several reservoir bottles. The drying system was composed of a freeze-dryer (Alpha 2–4; Martin Christ Gefriertrock nungsanlagen GmbH) and a vacuum pump (RZ 6; VACUUBRAND GMBH + CO KG).

Using these connected pieces of equipment (Fig. 1), the general procedure for fabricating the nanofibrous multichannel NCs was (1) assemble the different linkages of the mold system; (2) inject the polymer solution into the mold using a syringe; (3) regulate the cold trap to cool the mold using a programmed cooling process; (4) (a) cutoff the injection system, connect the lyophilization system, and freeze-dry the polymer scaffold; (b) exchange the solvent in the polymer gel with nonsolvent circulating through the peristaltic pump system [(a) or (b) was chosen according to the specific objectives]; (5) introduce, in order, the disinfectant (75% ethanol) and the rinsing solution; (6) add the growth factor solution or other functional molecular solution using the peristaltic pump system; (7) remove the mold and obtain the conduits. The procured NCs can be immediately used in cell culture or *in vivo* transplantation.

Fabrication of the NCs

Here, the mold applied for NCs structural parameter control has a mold cavity length of 6–8 cm, inner diameter of 3500 μm, and a wire-supporting hole number of 33. The diameter of Ni-Ti alloy wires is 200 μm.

NCs with a nanofibrous microstructure. PLLA was first dissolved in THF with a concentration of 60 mg/mL at 50°C, and the cold trap and mold were chilled to the preset temperature of −40°C via cold-oil external cycling. Using 60 mg/mL of PLLA solution to fabricate the conduit was based on the polymer content should be as low as possible (for degradation and porosity), but the mechanical strength of resultant conduit should meet the future demand of nerve implantation. The hot PLLA/THF solution was quickly injected into the cold mold using a syringe and the temperature of the system was maintained at −40°C for 2 h to induce the gelation and liquid–liquid (L-L) phase separation[34] of the polymer solution. Then, an infusion of cold ethanol (−40°C) followed by water (4°C) was completed for 2 h each using the peristaltic pump to replace the THF. After all the THF was replaced, the temperature of the cold trap was adjusted to −20°C, and then, the freeze-dryer was connected to the mold for 2 days. After intensive drying and mold removal, the NCs with a nano-fibrous microstructure (NNC) was obtained.

NCs with a ladder-like microstructure. PLLA was dissolved in dioxane with a concentration of 60 mg/mL at 50°C, and the mold system was precooled to −40°C. The hot PLLA/dioxane solution was quickly injected into the cold mold using a syringe and maintained at a temperature of −40°C for 2 h to induce a solid–liquid (S-L) phase separation[41] of the polymer solution. Then, the temperature of the cold trap was adjusted to −20°C, and the solvents were sublimated by a 2-day lyophilizing process. Finally, the mold was removed, and the NCs with a ladder-like microstructure (LNC) were obtained.

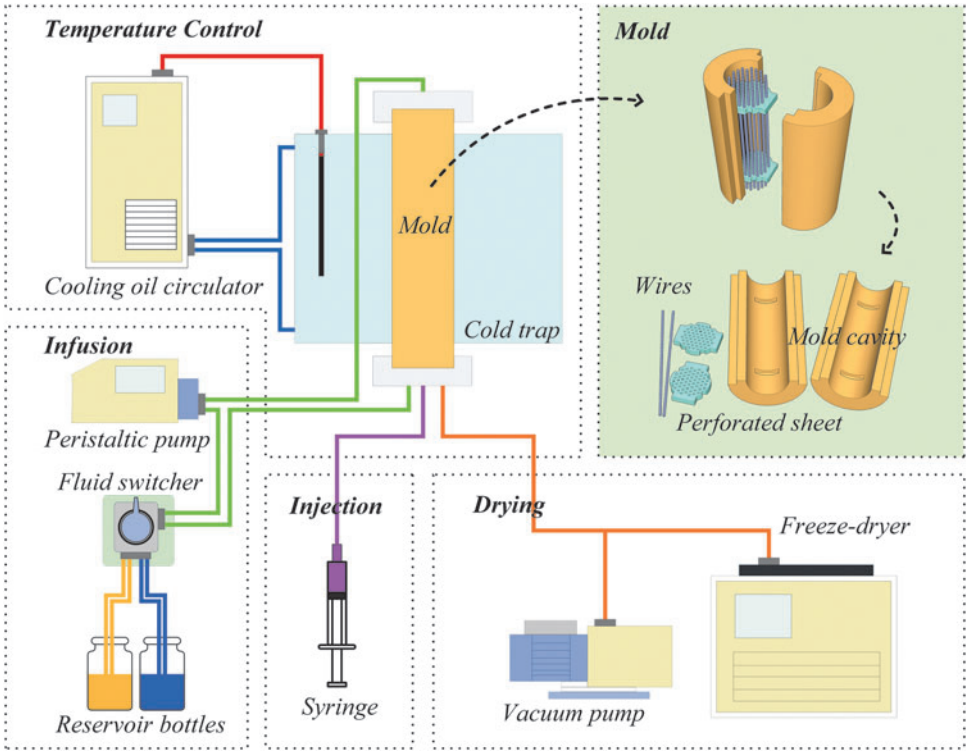

FIG. 1. Scheme of the systematized device for fabrication of polymeric conduits by combining injection molding and phase separation processes. The device includes several basic components: a temperature control system (a cooling oil circulator with an outer circulation thermocouple and a cold trap), an infusion system (a peristaltic pump, a fluid switcher, and reservoir bottles), an injection system (a syringe), a drying system (a vacuum pump and a freeze-dryer), the mold (two mold cavities, dozens of wires for channel formation, and two wire-supporting perforated sheets, the mold assembly is shown in the upper right corner of the diagram), and pipelines. Color images available online at www.liebertpub.com/tea

NCs with a macroporous and nano-wall microstructure. PLLA was dissolved in a dioxane–water mixture (88:12, v/v) with a concentration of 60 mg/mL at 50°C, and the mold system was precooled to 12°C. The hot PLLA/dioxane–water solution was injected into the cold mold, and the temperature was maintained at 12°C for 2 h to induce the gelation and L-L phase separation[42] of the polymer solution. Then, the temperature of the cold trap was adjusted to −20°C, and the mixed solvents were sublimated by a 2-day freeze-drying process, resulting in the NCs with a macrospherical pores and nano-fibrous pore walls (MNC).

Characterization of the NCs

The samples of NCs were quenched into liquid nitrogen and then snapped to create fracture surfaces. After coating with gold, the fracture surfaces were viewed with an SEM (JSM-6380LA Analytical Scanning Electron Microscope; JEOL LTD.) at 5 or 15 kV to observe the morphology. The representative images were selected to analyze the structural parameters (shown in Fig. 4) using image analysis software (ImageJ; National Institutes of Health), and the results were expressed as the mean ± standard deviation (SD) ($n = 10 \times 3 \times 3$, which means three samples were selected for each NCs, and three SEM micrographs were obtained for each sample. Ten measurement points were randomly selected in one SEM micrograph to calculate the sizes.).

The pore sizes and size distribution of NCs samples were determined by mercury porosimetry (PoreMaster 60; Quantachrome Corporation). Considering that the porosity was complementary to the ratio of the porous conduit weight to the theoretical solid conduit weight, the determination of the porosity for the three NCs was completed using the method described previously.[22] The porosity of the NCs includes two parts: the pores in the walls separating the open channels and the channels within the conduit. For the purpose of clarity, V_s is defined as the volume of the whole conduit, V_c as the volume of the channels, and V_w as the volume of walls; D and d are the diameters of the conduit and channels, respectively; l is the length of the conduit; and the number 33 is the number of channels; m is the mass of NC; ρ is the density of PLLA, which was 1.25 mg/mm^3. The relationship between these three factors is listed in Equation (1) as shown below. The quality of V_s and V_c is measured via Equation (2). Next, the porosity of the walls is given in the following Equation (3). Five samples for each NC were investigated to determine the porosity, and the results were expressed as the mean ± SD ($n = 5$).

$$V_w = V_s - V_c \tag{1}$$

$$V_s = \frac{\pi l}{4} D^2; \quad V_c = \frac{\pi l}{4} \times 33 \times d^2 \tag{2}$$

$$\text{Wall poresity } (\%) = \left(1 - \frac{m}{V_{w\rho}}\right) \times 100\% \tag{3}$$

The N_2-BET (Brunauer-Emmett-Teller) method was used to determine the specific surface areas of the porous conduits with a gas sorption instrument (ASAP-2020; Micromeritics Instrument Corporation). The conduit samples were degassed at 40°C for 8 h before analyses. The results were obtained by calculation via BET equation.

After the solvent removal procedure, BSA solution (100 μg/mL, in 0.1 M PBS, PH = 7.4) was infused into the conduits using the peristaltic pump and left to soak for 4 h to determine

the BSA adsorption efficiency of the conduits. Then, 15 mL of 0.1 M PBS (1 mL/min) was added to wash the free BSA from the conduit, and 50 mL of 1% (wt/v, mg/mL) sodium lauryl sulfate solution was circulated to elute the protein absorbed by the porous conduits. Eluent was collected for bicinchoninic acid protein assay. Five samples for each NC were investigated, and the results were expressed as the mean ± SD ($n = 5$).

The compression properties were determined using a KD-5 Electronic Pull Force Tester (Shenzhen Kaiqiangli Testing Instrument) at a crosshead speed of 0.5 mm/min at RT with a humidity of 50%. The NC samples were cut into cylindrical specimens of 5 mm in length before the test. Five samples were compressed between parallel plates using fully dried samples. The compression modulus was calculated according to the initial linear region of the stress-strain diagram by the slopes ($n = 5$).

The thermal properties of the conduits samples were measured on a differential scanning calorimeter (DSC, TA instruments MDSC 2910) under nitrogen atmosphere (40 mL/min). Three to 5 mg specimen was first heated from 0°C to 220°C at a heating rate of 10°C/min. The glass transition and melting endotherm were recorded as T_g and T_m, respectively. The intrinsic degree of crystallinity (X_c) was calculated according to Equation 4 shown below:

$$X_c = \frac{\Delta H_m}{\Delta H_m^o} \times 100\% \quad (4)$$

where ΔH_m is the enthalpy of melt peak in DSC curve and ΔH_m^o is the enthalpy of 100% crystalline polymer. For PLLA, $\Delta H_m^o = 203.4\ J/g$.[43]

NSCs seeding

Scaffold preparation for cell culture. Two experimental groups were established: without the NGF group (LNC, MNC, or NNC conduit only) and with the NGF group (LNC, MNC, or NNC conduit embedded with NGF, respectively). To obtain NGF-loaded conduit, we cut LNC, MNC, or NNC conduits into 2 mm rods, sterilized in 70% alcohol for 10 min, rinsed with sterile phosphate-buffered solution (PBS; pH 7.4) for 30 min, soaked in sterile NGF solution (10 mg/mL), stirred at 0°C for 6 h, and air-dried under laminar airflow overnight.

Cell culture and seeding. NSCs were prepared as described previously.[23,44] Briefly, 3- to 5-day-old Sprague–Dawley rat pups were anesthetized. Whole hippocampi were dissected and dissociated in the D-Hanks' balanced salt solution. After centrifuging at 1000 rpm for 5 min, the supernatant was removed. Pellet was resuspended in 5 mL basal medium, including DMEM/F12 (1:1) containing B27 supplement (20 mL/mL; Gibco) and bFGF (20 ng/mL; Invitrogen). The cells were plated onto 75-mL culture flasks. The medium was replaced every 3 days. Typically, the cells grew as suspending neurospheres and were passaged approximately once per week. NSCs from neurospheres were dissociated mechanically. Cells were then suspended in the basic medium (DMEM/F12 with 10% FBS) and seeded under two separate conditions: without the NGF group and with the NGF group. To seed neurospheres into the scaffold, we put 3.1×10^6 cells in 20 mL culture medium consisting of DMEM/F12 at a ratio of 1:1, 10% FBS, and 50 μg/mL ascorbic acid (Sigma-Aldrich) on the top of the conduit slice with Waterman filter paper (#1) beneath the slice to gently suck the cells into the channels and pores. Slices were incubated in 35-mm culture dishes for 14 days, with the culture medium replaced every 2 days.

Immunocytochemistry and statistical analysis. Differentiation of NSCs was determined using immunocytochemistry staining of cryosections, following standard protocol. Antibodies used in this section included mouse anti-Map2 (marker for neurons), rabbit anti-GFAP (marker for astrocytes), and mouse anti-O4 (marker for oligodendrocytes), followed by the incubation with secondary antibodies Cy3-conjugated anti-mouse or anti-rabbit IgG (Jackson Immunological Research). The section was examined under the Zeiss LSM 710 fluorescence microscope. For quantification of cell types in any given experiment, at least five random fields were selected and photographed (under the 20× lens). The percentage of positive cells was determined relative to the total number of DAPI-labeled (Invitrogen) cell nuclei. We counted ~500 cells in every group. Statistical analyses were performed using analysis of variance. The significance level was defined at 0.05.

Results

The morphologies and the microstructures of NCs

As illustrated in Figure 2, three types of NCs with 33 longitudinally aligned channels and different microstructures were successfully fabricated via L-L or S-L TIPS. The outer diameter of the conduit and the diameters of the channels in these NCs were not completely but closely equivalent to the inner cavity of the mold and the diameters of the Ni-Ti alloy wires (200 μm) (Table 1). Obvious shrinkage of MNC was generated using L-L phase separation and freeze-drying. In contrast, the volume change by swelling or shrinkage was minimal for NNC, which may be a result of the low temperature exchange of a poor solvent with a good solvent before freeze-drying. Additionally, the amount of the volume change observed in LNC was between the shrinkage observed for the MNC and NNC.

Although the general appearances of these three conduits were similar, their microstructures were considerably different. For the NNC, the THF was selected as the solvent for the PLLA, and the gelation temperature of the polymer solution was maintained at −40°C for 2 h in the process of the L-L TIPS. The cross-sectional SEM analysis of the sample showed a uniform nanofibrous network morphology between the adjacent channels, the fiber dimension was ~349 ± 167 nm, and the distances between nanofibers were in the range of 343 ± 183 nm. In the case of the MNC, a dioxane/water solution was used as the binary solvent for the PLLA to go through the L-L TIPS process at 12°C. Uniform micron-scale spherical pores (44.41 ± 7.15 μm) and approximate nanoscale fibrous walls were created inside. In contrast, a typical ladder-like morphology was observed in the cross-sectional SEM analysis of the LNC. In this system, dioxane was used as a solvent for the PLLA and the S-L TIPS process occurred at −40°C.

The physical properties of the multichannel conduits

These conduits had an approximate porosity of 92–94% (Fig. 3a), determined using gravimetry at room temperature,

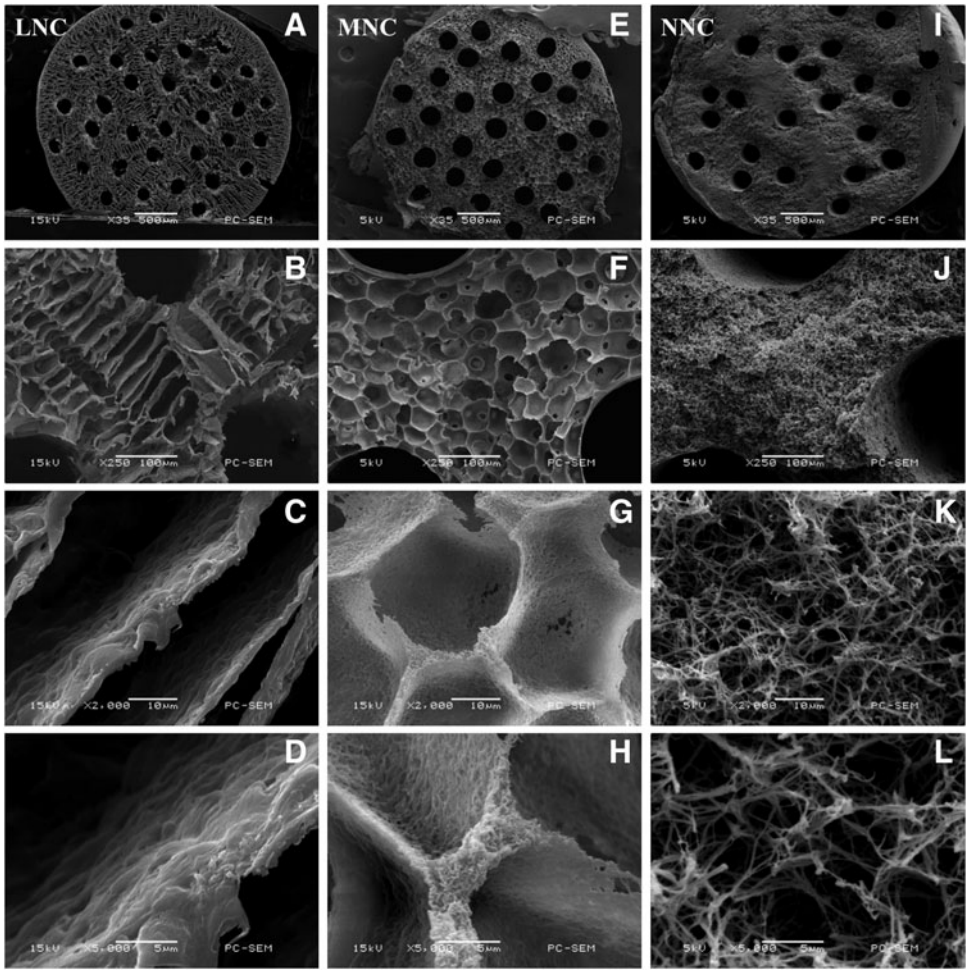

FIG. 2. SEM images of the conduits cross section using different magnification. (From left to right: LNC, MNC, and NNC; scale bar: 500 μm for **A, E, I**; 100 μm for **B, F, J**; 10 μm for **C, G, K**; and 5μm for **D, H, L**). NCs, nerve conduits; LNC, NCs with a ladder-like microstructure; MNC, NCs with a microspherical pores and nono-fibrous pore walls; NNC, NCs with a nanofibrous microstructure.

regardless of the detailed morphological features. It can be inferred that the porosities of the conduits depended primarily on the concentration of the polymer solution and was independent of the microstructure of the NCs. Furthermore, as shown in Figure 3b, the porosimetry analysis indicated that nearly 90% of the void space exhibited pore sizes in the range of 0.1 to 4.0 μm for the NNC, but the pore size range of the LNC increased from 3.5 to 15 μm. Two centers of pore size distribution of MNC (1.5 and 5.0 μm) were observed, which closed to the SEM observation. The specific surface area (Fig. 3c) of the NNC was 3.5 times more than that of the LNC and 2 times more than that of the MNC. Similarly, the adsorption of BSA (Fig. 3d) for the NNC was obviously higher than that of the MNC and LNC because of the higher specific surface area of NNC.

The compressive strength analysis indicated that the MNC was stiffer than the NNC and LNC (Fig. 4b) under compression. Moreover, a yield point (Fig. 4a) was observed for the NNC and MNC on the stress-strain curves. For the LNC, the compressive strength increased gradually with the increasing strain. From DSC curve (Fig. 5), melting peak of each sample appeared at 180.9°C for raw PLLA, 181.2°C for LNC, 179.7°C for MNC, and 179.7°C for NNC. X_c calculated from melting peak area was 20.6% for raw PLLA, 14.2% for LNC, 24.6% for MNC, and 27.8% for NNC.

The influences of the microstructure of the NCs on the differentiation of the NSCs

To evaluate the influences of the microstructure of the NCs on the nerve cells behaviors, and considering that the NSCs were often used to transplant for the repair of spinal cord injury, we inspected the differentiation of the NSCs seeded into the conduits in the culture medium containing NGF or not. The NSCs were stained with three different cell type markers, and the differentiation of NSCs into neural cells types was demonstrated, that is, neurons (red in Fig. 6A–F, arrow), astrocytes (see arrow in Fig. 7A–F), and oligodendrocytes (see arrow in Fig. 8A–F). At day 14, in the no NGF group, only 15.76% of 598 counted cells were Map2 positive in the LNC scaffold (Fig. 6A), as were 23.29% of 574 in the MNC scaffold (Fig. 6B) and 31.32% of 673 in the NNC scaffold (Fig. 6C). Differently, the Map2-positive cells were significantly increased to 68.21%, 73.46%, and 81.11% in the LNC, MNC, and NNC groups in the NGF groups, respectively (Table 2). GFAP-positive astrocytes (Fig. 7) and O_4-positive oligodendrocytes (Fig. 8) were also examined. Percentage of GFAP-positive cells was the lowest in NNC either with NGF or without NGF, as compared with other groups (data not shown). However, the ratio of O_4-positive cells was not different between without NGF and with NGF group (data not shown).

Table 1. Thermal-Induced Phase Separation Condition and Structural Parameters of the Three Different Conduits

	LNC	*MNC*	*NNC*
Solvent	DOX	Mixture[a]	THF
Endpoint temperature (°C)	−40	12	−40
Solvent removal	Freeze-drying	Freeze-drying	Exchange-drying
Length of conduit (cm)	6–8	6–8	6–8
$NO_{channel}$[b]	33	33	33
$\bar{\phi}_{out}$ (μm)[c]	3158 ± 33	2867 ± 29	3619 ± 111
$\bar{\phi}_{channel}$ (μm)[d]	176 ± 17	246 ± 13	225 ± 19
$\bar{d}_{channel}$[e]	424 ± 77	461 ± 33	485 ± 128
$\bar{d}_{layers}$ (μm)[f]	22.63 ± 8.01	—	—
$\bar{h}_{layer}$ (μm)[g]	2.03 ± 0.33	—	—
$\bar{\phi}_{pore}$ (μm)[h]	—	44.41 ± 7.15	—
$\bar{d}_{pores}$ (μm)[i]	—	39.14 ± 6.61	—
$\bar{\phi}_{fiber}$ (nm)[j]	—	—	349 ± 167
$\bar{d}_{fibers}$ (nm)[k]	—	—	343 ± 183

[a]DOX and water mixed solvent, 88:12 (v/v).
[b]Number of channel.
[c]Average outer diameter of conduits.
[d]Average diameter of channels.
[e]Average center distance of adjacent channels.
[f]Average distance of adjacent layers.
[g]Average thickness of layers.
[h]Average diameter of the spherical pores.
[i]Average center distance of adjacent pores.
[j]Average diameter of the fibers.
[k]Average distance of adjacent fibers.

Structural parameter data were obtained by the analysis of the SEM images using image analysis software (ImageJ; National Institutes of Health), and the results were expressed as the mean ± standard deviation ($n = 10 \times 3 \times 3$, 10 random sites, 3 images, 3 samples).

NCs, nerve conduits; LNC, NCs with ladder-like microstructure; MNCs, NCs with microspherical pores and nano-fibrous pore walls; NNCs, NCs with a nano-fibrous microstructure.

Discussion

In our previous work,[22] we devised a protocol for the fabrication of poly(lactide-co-glycolide) (PLGA) multichannel conduits with hierarchical pore architectures, including 16 longitudinally aligned channels with 500–1000 μm diameters, 100–200 μm macropores, and 20–50 μm micropores. The method integrated low temperature injection, S-L phase separation, and salt-leaching technologies. The limitations of this method were focused on the larger diameter of

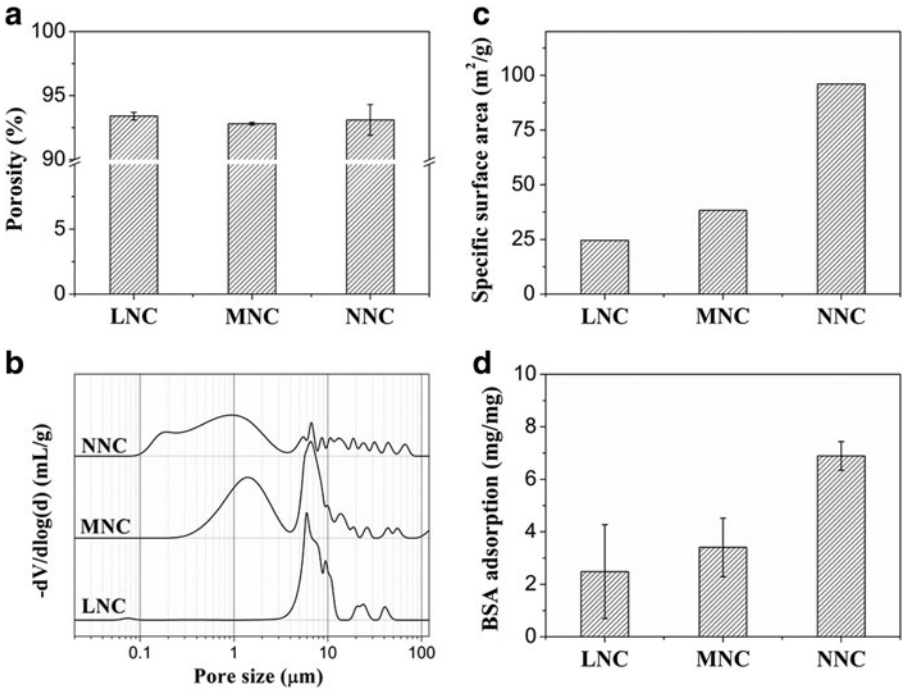

FIG. 3. Porosity **(a)**, pore size distribution **(b)**, specific surface area **(c),** and bovine serum albumin adsorption **(d)** of the conduit samples.

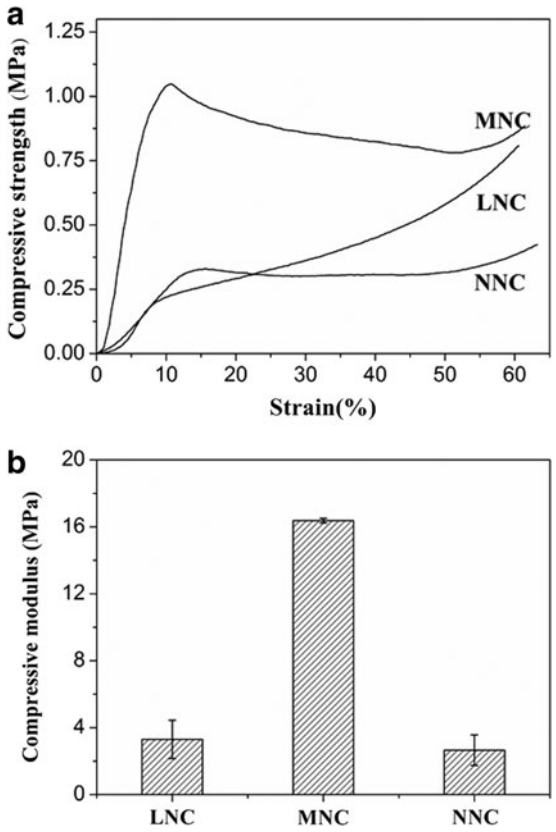

FIG. 4. Stress-strain curves (**a**) and compressive modulus (**b**) of conduit samples.

the channel and the inconvenience of the controlled process of phase separation. Here, we designed a systematized device (Fig. 1), fabricated NCs with 33 aligned channels with a 200 μm diameter, and with different microstructures by controlling various phase separation processes, such as L-L phase separation in a tetrahydrofuran or dioxane/water solution and S-L phase separation in dioxane. Therefore, the

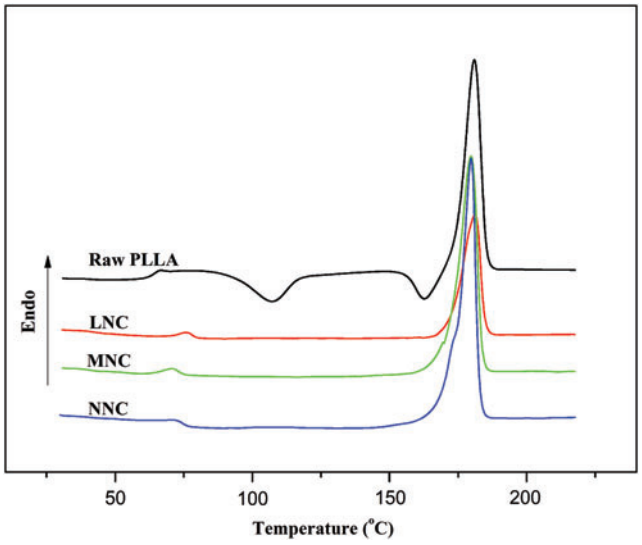

FIG. 5. The first-heat thermogram of differential scanning calorimeter of conduit samples. PLLA, poly(L-lactide) Color images available online at www.liebertpub.com/tea

multichannel NCs with a nanofibrous network, spherical micropores, nanofibrous pores wall, and ladder-like pores were obtained.

Several points in the fabrication process of these NCs with different precise microstructures are particularly worthy of notice. First, in the design of the mold, the Ti-Ni wires were drilled through two wire-supporting perforated sheets, which were fixed on the pegs of the mold. Unlike our previous work, we adopted a cold trap to control the temperature of the mold. Therefore, to convert the various phase separation conditions, it was possible to use different sources for the cooling mediums, for example, silicone oil, liquid nitrogen, dry ice, alcohol, water, and so on. Moreover, with the flexibility of this system, other 3D scaffolds with different complex outer appearances and inner microstructures can also be fabricated by altering the specific design of the mold. In addition, the sprue, exhaust parts, leak proof seal, and the entire mold should be precisely machined, and the lumen of the mold should be flashed to a convenient demolding. Second, it is important to convert the mold temperature to a selected value as soon as possible and to maintain a constant temperature accurately using the controllable heat transfer efficiency and real-time temperature monitor because the thermal histories of the polymer solution throughout the TIPS process directly affected the final morphologies of the resulting scaffolds. As reported in our previous work[43] and Ma's studies,[41,42] the gelation temperature of the PLLA/THF or the PLLA/dioxane-water solution and the cooling rates of the systems determined the sizes of the PLLA microcrystals. The slow cooling often induced an increase in the degree of crystallinity and an increase in the microcrystallite domain size, which would result in an appearance of the coalescence of nanofibers and plate-like structures. Third, to ensure the stability of the scaffold by decreasing the shrinkage or swelling of the final product, the solvent exchange was incorporated using an infusion system after the TIPS process. This system can also be used as a method to measure the conduit permeability by monitoring the pressure changes between two sides of the conduit. Additionally, it provided a convenient method for introducing biological molecules through the peristaltic pump dynamic loading of functional biomolecules via physical adsorption in a low microthermal environment. Finally, the mold installation, immobilization, and removal were easy to operate throughout the entire process, which is beneficial for obtaining the neural conduits or other scaffolds.

By utilizing this systematized device, we fabricated three types of 33-channel PLLA NCs: NCs with a nano-fibrous microstructure (NNC), NCs with a microspherical pores and nano-fibrous pore walls (MNC), and NCs with a ladder-like microstructure (LNC). The NNC showed a typical nanofibrous microstructure similar to those reported in Ma's work,[41,42] in which the PLLA/THF system went through the L-L phase separation process at −40°C for 2 h gelation. The MNC was fabricated from PLLA in a mixed solvent (dioxane/water 88/12) using an L-L phase separation and gelling process at 12°C for 2 h. The homogeneous micropores formed when the nonsolvent water was incorporated, which corresponds to an increase in the coarsening depth. Here, the gelation temperature, quenching depth (the proportion of nonsolvent in the mixture solution system), and the coarsening time (gelation time) were selected according to our

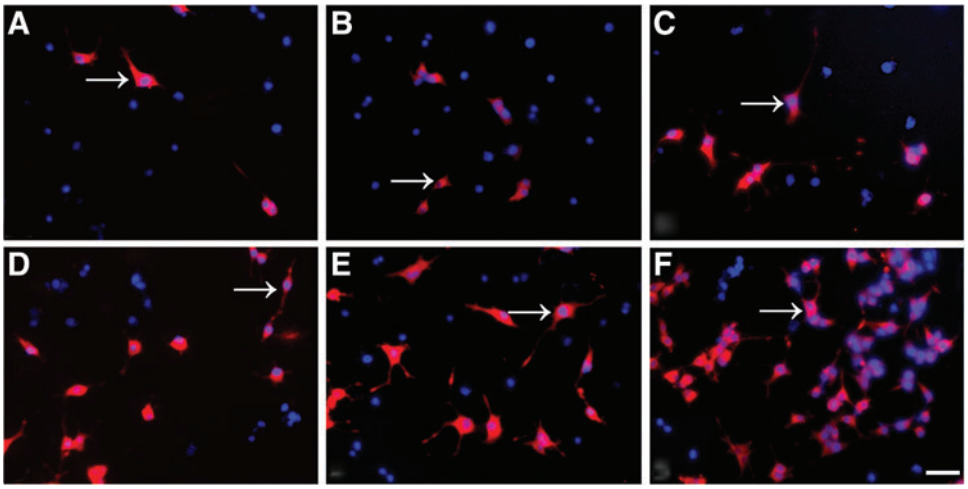

FIG. 6. Fluorescence micrograph of the NSCs seeded on the nerve conduits showing the Map2 positively stained cells. NSCs were cultured in the without NGF and with NGF group for 14 days, respectively. Cells were immunostained in **(A)** LNC only; **(B)** MNC only; **(C)** NNC only; **(D)** LNC-loaded NGF; **(E)** MNC-loaded NGF; **(F)** NNC-loaded NGF group with markers for neurons (Map2; arrow; red). Either in the without NGF or with NGF group, the positively stained cells ($Map2^+$) were higher in the NNC scaffold compared with other rods in the same group ($p<0.05$; $n=3$ for each group). The percentage of Map2-positive cells was highest in the NGF-loaded N rods compared with any other rods. Nuclei were stained by DAPI (blue). Scale bar = 20 μm in **A–F**. NSC, nerve stem cells. Color images available online at www.liebertpub.com/tea

previous work.[43] The LNC was similar to the ladder-like porous microstructure of the PLGA in our previous work.[22] Because of these disparate architectures, the specific surface area and the adsorption capacity of BSA for the NNC group were enhanced significantly compared to that of the MMC and LNC groups (as shown in Fig. 3). These results were consistent with the SEM images and the porosities of the scaffolds.

The analysis of the compressive performance showed the appearance of yield points in the stress-strain curves for the NNC and MNC groups, which may be attributable to the collapse of the pores, particularly for the NNC. The DSC measurement showed a high crystallinity for the PLLA (27.8%), but 24.6% for the MNC and 14.2% for the LNC. This relative high crystallinity made the porous scaffold more brittle. However, the higher compressive strength of the MMC should be ascribed to its special spherical porous structure. The low mechanical strength of the NNC should be enhanced for future use.

Many studies have reported that the nanoscale fiber affected neural cell proliferation, attachment, and neurite outgrowth.[45–48] The physical cue formed by this topology has also been introduced in the inner lumen of single-channel NCs to improve axonal growth guidance with some success.[26,27,31,32] It has been reported that micro- and nanostructural features can effectively induce neuronal differentiation of stem cells, including embryonic stem cells,[37,49] mesenchymal stem cells,[50] and NSCs.[51] As a general strategy for neural tissue engineering, stem cell-based therapy shows a significant potential by replenishing the neurons after implant and differentiation. Using the microstructure of a scaffold to regulate the differentiation of seeded NSCs is a feasible route. Obviously, the estimation on the oriented differentiation of stem cells into neurons in a 3D microenvironment *in vitro* will be closer to an *in vivo* scenario. However, there are few studies on neuronal differentiation of stem cells in the micro- and nanostructural 3D neural scaffolds, particularly multichannel conduits, which have the great potential in nerve tissue engineering. It is necessary to study the neuronal differentiation of NSCs in these three multichannel conduits with precisely controlled pores and nanofibrous structure.

In this study, we examined whether the microstructure of the conduits would direct the differentiation of NSCs into neurons. By mimicking the structure of the natural extracellular matrix, the NNC group exhibited obvious advantages in promoting the NSCs differentiation into neurons compared to the MNC and LNC groups. The percentage of astrocytes was reduced when the NSCs were seeded onto the NNC compared to the MNC and LNC.

Furthermore, due to the ultrahigh specific surface area, NGF adsorbed NNC can dramatically promote the level of NSC-oriented differentiation to neurons. In our *in vitro* investigation, NNC functionalized by simply adsorption of NGF led to the 81.11% of neurons derived from the differentiation of the seeded NSCs. This exciting result reflected the advance of the nanofibrous microstructure of NNC in the potential application in neural tissue engineering.

Table 2. Comparison of Map2-Positive Cells (Mean ± Standard Deviation, %) Between Two Groups

Groups	n	*Without NGF*	*With NGF*
LNC	3	15.76 ± 3.27^a	68.21 ± 4.37^d
MNC	3	23.29 ± 4.65^b	73.46 ± 4.11^e
NNC	3	31.12 ± 3.98^c	81.11 ± 2.16^f

One-way analysis of variance test was used to show the statistical difference.

$p<0.05$: a versus b; a versus c; b versus c; d versus e; d versus f; e versus f; a versus d; b versus e; c versus f.

LNC, NCs with a ladder-like microstructure; MNC, NCs with a microspherical pores and nano-fibrous pore walls; NNC, NCs with a nano-fibrous microstructure

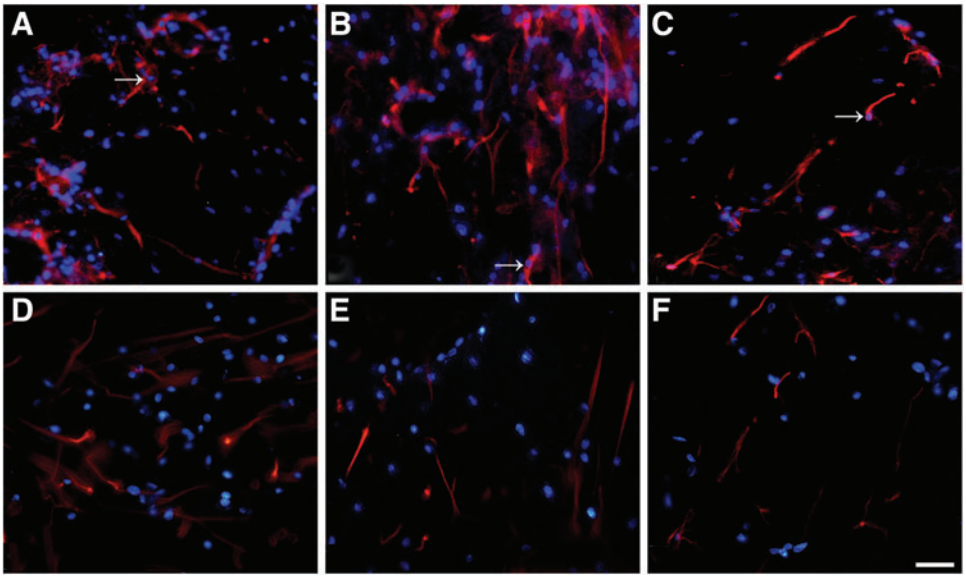

FIG. 7. Fluorescence micrograph of the NSCs seeded on the nerve conduits showing the GFAP positively stained cells. NSCs were cultured in the scaffolds for 14 days. Cells were immunostained in **(A)** LNC only; **(B)** MNC only; **(C)** NNC only; **(D)** LNC-loaded NGF; **(E)** MNC-loaded NGF; **(F)** NNC-loaded NGF group with markers for astrocytes (GFAP; arrow; red). Percentage of GFAP-positive cells was the lowest in NNC rods either in the without NGF group **(C)** or in the with NGF group **(F)** compared with other rods. In contrast, astrocytes were abundant in the LNC scaffold **(A, D)** and MNC scaffold **(B, E)**. Nuclei were stained by DAPI (blue). Scale bar = 20 μm in **A–F**. Color images available online at www.liebertpub.com/tea

However, the mechanisms of differentiation induced by physical cues are still poorly understood.[2] Some researchers proposed that the elongation of the cytoskeleton during cell culture on the substrate with nano-features will result in a transfer of tensile force to the nuclei, influencing gene expression and signal transduction.[52] We supposed that the multichannel conduits with nanofibrous microstructure closely matched the structure of the natural nerve and highlighted the specific surface area and adsorption capacity of proteins, and more functional biomolecules (e.g., growth factors) could be adsorbed into the NNC scaffold when incubating cells. It would provide a more realistic 3D microenvironment for nerve cells to proliferate and differentiate irrespective of *in vitro* or *in vivo*.

Conclusion

Three multichannel NCs with nanofibrous microstructures were fabricated using a systematic device developed by our group. The number of channels and the defined features inside the conduit can be constructed easily by controlling the phase separation parameters in different polymer solutions. In the case of with/without neurotrophic factors, the nanofibrous structure in a neural scaffold can enhance the NSCs differentiation into

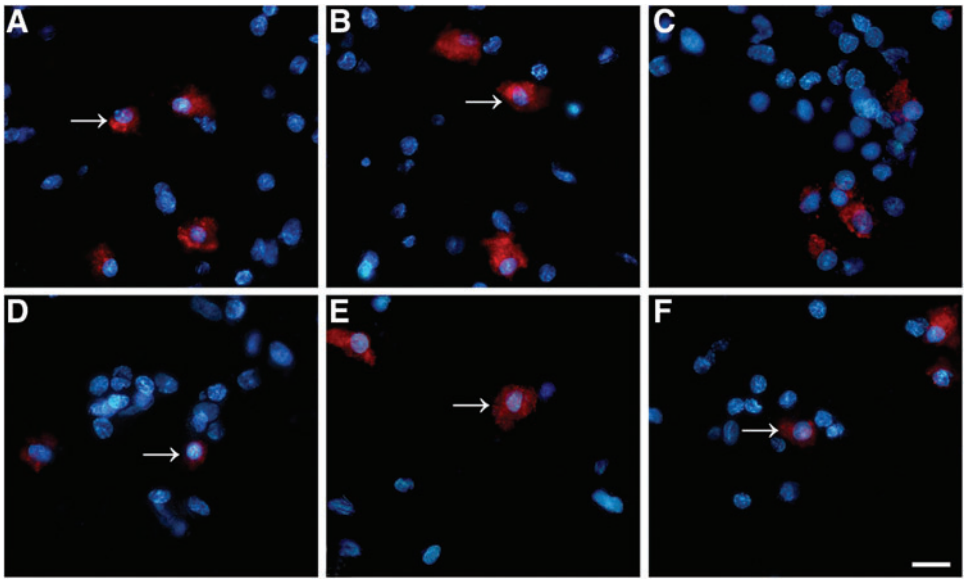

FIG. 8. Fluorescence micrograph of the NSCs seeded on the nerve conduits showing the O_4 positively stained cells. NSCs were cultured in the scaffolds for 14 days. Cells were immunostained in **(A)** LNC only; **(B)** MNC only; **(C)** NNC only; **(D)** LNC-loaded NGF; **(E)** MNC-loaded NGF; **(F)** NNC-loaded NGF group with markers for oligodendrocytes (O_4; arrow; red). The ratio of O_4-positive cells was not different between the without NGF and with NGF groups. Nuclei were stained by DAPI (blue). Scale bar = 20 μm in **A–F**. Color images available online at www.liebertpub.com/tea

neurons. This result may contribute to the high specific surface area and the adsorption capacity of the proteins of the nanofibrous structure. More details are still under investigation.

Acknowledgments

The authors acknowledge the financial support from the National Natural Science Foundation of China (Grants 5107378, 20974128 and U1134007) and the Emphasis Foundation of Social Developmental Field of Guangdong Province (No. 2011A030300004).

Disclosure Statement

No competing financial interests exist.

References

1. Schmidt, C.E., and Leach, J.B. Neuraltissue engineering: strategies for repair and regeneration. Annu Rev Biomed Eng **5,** 293, 2003.
2. Hoffman, K.D., Mitchel, J.A., and Bellamkonda, R.V. Topography, Cell Response, and Nerve Regeneration. In: Yarmush, M.L., Duncan, J.S., and Gray, M.L., eds. Annual Review of Biomedical Engineering, Vol. 12. Palo Alto: Annual Reviews, p. 203, 2010.
3. Gu, X., Ding, F., Yang, Y., and Liu, J. Construction of tissue engineered nerve grafts and their application in peripheral nerve regeneration. Prog Neurobiol **93,** 204, 2011.
4. Khainga, Z.Z., and Schmidta, C.E. Advances in natural biomaterials for nerve tissue repair. Neurosci Lett **519,** 103, 2012.
5. Spivey, E.C., Khaing, Z.Z., Shear, J.B., and Schmidt, C.E. The fundamental role of subcellular topography in peripheral nerve repair therapies. Biomaterials **33,** 4264, 2012.
6. Kehoe, S., Zhang, X.F., and Boyd, D. FDA approved guidance conduits and wraps for peripheral nerve injury: a review of materials and efficacy. Injury **43,** 553, 2012.
7. Georgiou, M., Bunting, S.C.J., Davies, H.A., Loughlin, A.J., Golding, J.P., and Phillips, J.B. Engineered neural tissue for peripheral nerve repair. Biomaterials **34,** 7335, 2013.
8. Widmer, M.S., Gupta, P.K., Lu, L., Meszlenyi, R.K., Evans, G.R.D., Brandt, K., Savel, T., Gurlek, A., Patrick, C.W., Jr., and Mikos, A.G. Manufacture of porous biodegradable polymer conduits by an extrusion process for guided tissue regeneration. Biomaterials **19,** 1945, 1998.
9. Evans, G.R.D., Brandt, K., Widmer, M.S., Lu, L., Meszlenyi, R.K., Gupta, P.K., Mikos, A.G., Hodges, J., William, J., Gurlek, A., Nabawi, A., Lohman, R., and Patrick, C.W., Jr. *In vivo* evaluation of poly(L-lactic acid) porous conduits for peripheral nerve regeneration. Biomaterials **20,** 1109, 1999.
10. Yang, Y., Gu, X., Tan, R., Hu, W., Wang, X., Zhang, P., and Zhang, T. Fabrication and properties of a porous chitin/chitosan conduit for nerve regeneration. Biotechnol Lett **26,** 1793, 2004.
11. Tang, S., Zhu, J., Xu, Y., Xiang, A.P., Jiang, M.H., and Quan, D. The effects of gradients of nerve growth factor immobilized PCLA scaffolds on neurite outgrowth *in vitro* and peripheral nerve regeneration in rats. Biomaterials **34,** 7986, 2013.
12. Hadlock, T., Sundback, C., Hunter, D., Cheney, M., and Vacanti, J.P. A polymer foam conduit seeded with Schwann cells promotes guided peripheral nerve regeneration. Tissue Eng **6,** 119, 2000.
13. Sundback, C., Hadlock, T., Cheney, M., and Vacanti, J. Manufacture of porous polymer nerve conduits by a novel low-pressure injection molding process. Biomaterials **24,** 819, 2003.
14. Bender, M.D., Bennett, J.M., Waddell, R.L., Doctor, J.S., and Marra, K.G. Multi-channeled biodegradable polymer/CultiSpher composite nerve guides. Biomaterials **25,** 1269, 2004.
15. Huang, Y.C., Huang, Y.Y., Huang, C.C., and Liu, H.C. Manufacture of porous polymer nerve conduits through a lyophilizing and wire-heating process. J Biomed Mater Res B Appl Biomater **74B,** 659, 2005.
16. Yu, T.T., and Shoichet, M.S. Guided cell adhesion and outgrowth in peptide-modified channels for neural tissue engineering. Biomaterials **26,** 1507, 2005.
17. Yang, Y., Delaporte, L., Rives, C., Jang, J., Lin, W., Shull, K., and Shea, L.D. Neurotrophin releasing single and multiple lumen nerve conduits. J Control Release **104,** 433, 2005.
18. Moore, M.J., Friedman, J.A., Lewellyn, E.B., Mantila, S.M., Krych, A.J., Ameenuddin, S., Knight, A.M., Lu, L., Currier, B.L., Spinner, R.J., Marsh, R.W., Windebank, A.J., and Yaszemski, M.J. Multiple-channel scaffolds to promote spinal cord axon regeneration. Biomaterials **27,** 419, 2006.
19. Wang, A., Ao, Q., Cao, W., Yu, M., He, Q., Kong, L., Zhang, L., Gong, Y., and Zhang, X. Porous chitosan tubular scaffolds with knitted outer wall and controllable inner structure for nerve tissue engineering. J Biomed Mater Res A **79A,** 36, 2006.
20. Yao, L., Billiar, K.L., Windebank, A.J., and Pandit, A. Multichanneled collagen conduits for peripheral nerve regeneration: design, fabrication, and characterization. Tissue Eng Part C Methods **16,** 1585, 2010.
21. Tansey, K.E., Seifert, J.L., Botterman, B., Delgado, M.R., and Romero, M.I. Peripheral nerve repair through multiluminal biosynthetic implants. Ann Biomed Eng **39,** 1815, 2011.
22. He, L., Zhang, Y., Zeng, C., Ngiam, M., Liao, S., Quan, D., Zeng, Y., Lu, J., and Ramakrishna, S. Manufacture of PLGA multiple-channel conduits with precise hierarchical pore architectures and *in vitro*/*vivo* evaluation for spinal cord injury. Tissue Eng Part C Methods **15,** 243, 2009.
23. Xiong, Y., Zeng, Y.S., Zeng, C.G., Du, B.L., He, L.M., Quan, D.P., Zhang, W., Wang, J.M., Wu, J.L., Li, Y., and Li, J. Synaptic transmission of neural stem cells seeded in 3-dimensional PLGA scaffolds. Biomaterials **30,** 3711, 2009.
24. Li, G.N., and Hoffman-Kim, D. Tissue-engineered platforms of axon guidance. Tissue Eng Part B Rev **14,** 33, 2008.
25. Piotrowicz, A., and Shoichet, M.S. Nerve guidance channels as drug delivery vehicles. Biomaterials **27,** 2018, 2006.
26. Bhattarai, N., Li, Z.S., Gunn, J., Leung, M., Cooper, A., Edmondson, D., Veiseh, O., Chen, M.H., Zhang, Y., Ellenbogen, R.G., and Zhang, M. Natural-synthetic polyblend nanofibers for biomedical applications. Adv Mater **21,** 2792, 2009.
27. Yao, L., O'Brien, N., Windebank, A., and Pandit, A. Orienting neurite growth in electrospun fibrous neural conduits. J Biomed Mater Res B **90B,** 483, 2009.
28. Zhu, Y., Wang, A., Patel, S., Kurpinski, K., Diao, E., Bao, X., Kwong, G., Young, W.L., and Li, S. Engineering bilayer nanofibrous conduits for peripheral nerve regeneration. Tissue Eng Part C Methods **17,** 705, 2011.

29. Lacour, S.P., Atta, R., FitzGerald, J.J., Blamire, M., Tarte, E., and Fawcett, J. Polyimide micro-channel arrays for peripheral nerve regenerative implants. Sensors Actuators A Phys **147,** 456, 2008.
30. Valmikinathan, C.M., Tian, J., Wang, J., and Yu, X. Novel nanofibrous spiral scaffolds for neural tissue engineering. J Neural Eng **5,** 422, 2008.
31. Papenburg, B.J., Liu, J., Higuera, G.A., Barradas, A.M.C., de Boer, J., van Blitterswijk, C.A., Wessling, M., and Stamatialis, D. Development and analysis of multi-layer scaffolds for tissue engineering. Biomaterials **30,** 6228, 2009.
32. Yucel, D., Kose, G.T., and Hasirci, V. Polyester based nerve guidance conduit design. Biomaterials **31,** 1596, 2010.
33. Oh, S.H., Kim, J.H., Song, K.S., Jeon, B.H., Yoon, J.H., Seo, T.B., Namgung, U., Lee, I.W., and Lee, J.H. Peripheral nerve regeneration within an asymmetrically porous PLGA/Pluronic F127 nerve guide conduit. Biomaterials **29,** 1601, 2008.
34. Yang, F., Murugan, R., Wang, S., and Ramakrishna. S. Electrospinning of nano/micro scale poly(L-lactic acid) aligned fibers and their potential in neural tissue engineering. Biomaterials **26,** 2603, 2005.
35. Koh, H.S., Yong, T., Chan, C.K., and Ramakrishna, S. Enhancement of neurite outgrowth using nano-structured scaffolds coupled with laminin. Biomaterials **29,** 3574, 2008.
36. Lee, J.Y., Bashur, C.A., Goldstein, A.S., and Schmidt, C.E. Polypyrrole-coated electrospun PLGA nanofibers for neural tissue applications. Biomaterials **30,** 4325, 2009.
37. Xie, J.W., MacEwan, M.R., Li, X.R., Sakiyama-Elbert, S.E., and Xia, Y.N. Neurite outgrowth on nanofiber scaffolds with different orders, structures, and surface properties. ACS Nano **3,** 1151, 2009.
38. Ma, P.X., and Zhang, R. Synthetic nano-scale fibrous extracellular matrix. J Biomed Mater Res **46,** 60, 1999.
39. Sun, C.H., Jin, X.B., Holzwarth, J.M., Liu, X.H., Hu, J., Gupte, M.J., Zhao, Y.M., and Ma, P.X. Development of channeled nanofibrous scaffolds for oriented tissue engineering. Macromol Biosci **12,** 761, 2012.
40. Chen, V.J., and Ma, P.X. The effect of surface area on the degradation rate of nano-fibrous poly(L-lactic acid) foams. Biomaterials **27,** 3708, 2006.
41. Zhang, R.Y., and Ma, P.X. Porous poly(L-lactic acid)/apatite composites created by biomimetic process. J Biomed Mater Res **45,** 285, 1999.
42. Wei, G., and Ma, P.X. Structure and properties of nano-hydroxyapatite/polymer composite scaffolds for bone tissue engineering. Biomaterials **25,** 4749, 2004.
43. He, L.M., Zhang, Y.Q., Zeng, X., Quan, D.P., Liao, S., Zeng, Y.S., Lu, J., and Ramakrishna, S. Fabrication and characterization of poly(L-lactic acid) 3D nanofibrous scaffolds with controlled architecture by liquid-liquid phase separation from a ternary polymer-solvent system. Polymer **50,** 4128, 2009.
44. Zeng, Y.S., Ding, Y., Wu, L.Z., Guo, J.S., Li, H.B., Wong, W.M., *et al.* Co-transplantation of Schwann cells promotes the survival and differentiation of neural stem cells transplanted into the injured spinal cord. Dev Neurosci **27,** 20, 2005.
45. Seidlits, S.K., Lee, J.Y., and Schmidt, C.E. Nanostructured scaffolds for neural applications. Nanomedicine (Lond) **3,** 183, 2008.
46. Kolind, K., Leong, K.W., Besenbacher, F., and Foss, M. Guidance of stem cell fate on 2D patterned surface. Bimaterials **33,** 6626, 2012.
47. Zhao, C., Tan, A., Pastrin, G., and Ho, H.K. Nanomaterial scaffolds for stem cell proliferation and differentiation in tissue engineering. Biotechnol Adv **31,** 654, 2013.
48. Wagers, A.J. The stem cell niche in regenerative medicine. Cell Stem Cell **10,** 362, 2012.
49. Lee, M.R., Kwon, K.W., Jung, H., Kim, H.N., Suh, K.Y., Kim, K., and Kim, K.S. Direct differentiation of human embryonic stem cells into selective neurons on nanoscale ridge/groove pattern arrays. Biomaterials **31,** 4360, 2010.
50. Yim, E.K., Pang, S.W., and Leong, K.W. Synthetic nanostructures inducing differentiation of human mesenchymal stem cells into neuronal lineage. Exp Cell Res **313,** 1820, 2007.
51. Christopherson, G.T., Song, H., and Mao, H.Q. The influence of fiber diameter of electrospun substrates on neural stem cell differentiation and proliferation. Biomaterials **30,** 556, 2009.
52. Bettinger, C.J., Langer, R., and Borenstein, J.T. Engineering substrate topography at the micro- and nanoscale to control cell function. Angew Chem Int Ed Engl **48,** 5406, 2009.

Address correspondence to:
Daping Quan, PhD
DSAPM and PCFM Lab
School of Chemistry and Chemical Engineering
Sun Yat-Sen University
135 Xin'gang Xi Road
Guangzhou 510275
China

E-mail: cesqdp@mail.sysu.edu.cn

Received: May 10, 2013
Accepted: October 15, 2013
Online Publication Date: January 24, 2014